Parameter-Free Adaptive Multi-Scale Channel-Spatial Attention Aggregation framework for 3D Indoor Semantic Scene Completion Toward Assisting Visually Impaired⋆

Qi He[a], XiangXiang Wang[a,b,e,*], Jingtao Zhang[c], Yongbin Yu[a,*], Hongxiang Chu[f], Manping Fan[a], JingYe Cai[a] and Zhenglin Yang[b,c,*]

[a]School of Information and Software Engineering, University of Electronic Science and Technology of China, Chengdu, Sichuan, China
[b]Sichuan Provincial Key Laboratory for Human Disease Gene Study, Sichuan Academy of Medical Sciences & Sichuan Provincial People's Hospital, University of Electronic Science and Technology of China, Chengdu, Sichuan, China
[c]School of Medicine, University of Electronic Science and Technology of China, Chengdu, Sichuan, China
[d]Research Unit for Blindness Prevention, Chinese Academy of Medical Sciences, Sichuan Academy of Medical Sciences and Sichuan Provincial People's Hospital, Chengdu, Sichuan, China
[e]Tibetan Language Intelligence National Key Laboratory, Qinghai Normal University, Xining, Qinghai, China
[f]Department of Scientific Research, Zibo Normal College, Zibo, Shandong, China

ARTICLE INFO

Keywords:
3D Semantic Scene Completion
3D Occupancy Prediction
Attention Mechanism
Visually Impaired Assistance
Indoor Navigation

ABSTRACT

In indoor assistive perception for visually impaired users, 3D Semantic Scene Completion (SSC) is expected to provide structurally coherent and semantically consistent occupancy under strictly monocular vision for safety-critical scene understanding. However, existing monocular SSC approaches often lack explicit modeling of voxel-feature reliability and regulated cross-scale information propagation during 2D–3D projection and multi-scale fusion, making them vulnerable to projection diffusion and feature entanglement and thus limiting structural stability.To address these challenges, this paper presents an Adaptive Multi-scale Attention Aggregation (AMAA) framework built upon the MonoScene pipeline. Rather than introducing a heavier backbone, AMAA focuses on reliability-oriented feature regulation within a monocular SSC framework. Specifically, lifted voxel features are jointly calibrated in semantic and spatial dimensions through parallel channel–spatial attention aggregation, while multi-scale encoder–decoder fusion is stabilized via a hierarchical adaptive feature-gating strategy that regulates information injection across scales.Experiments on the NYUv2 benchmark demonstrate consistent improvements over MonoScene without significantly increasing system complexity: AMAA achieves 27.25% SSC mIoU (+0.31) and 43.10% SC IoU (+0.59). In addition, system-level deployment on an NVIDIA Jetson platform verifies that the complete AMAA framework can be executed stably on embedded hardware. Overall, AMAA improves monocular SSC quality and provides a reliable and deployable perception framework for indoor assistive systems targeting visually impaired users.

1. Introduction

Visual impairment affects a large global population and remains a major barrier to independent mobility and daily living. According to the World Health Organization (WHO), at least 2.2 billion people worldwide experience vision impairment or blindness, underscoring the urgent societal demand for reliable and accessible assistive perception technologies [1]. Although indoor environments such as homes, offices, and public buildings are spatially bounded, they are often characterized by dense object distributions, heterogeneous layouts, frequent occlusions, and dynamic changes [2]. For visually impaired users, the lack of continuous and reliable spatial awareness in such environments substantially increases the risk of collisions and falls. Consequently, the trade-off between environmental understanding quality and system burden has become a central consideration in the design of assistive perception systems intended for long-term daily use [3, 4].

From a task perspective, indoor assistance requires more than recognizing object categories; it critically depends on modeling 3D occupancy and structural relationships of the surrounding environment. Inaccurate or fragmented geometric representations can directly compromise the safety and reliability of obstacle avoidance and downstream decision making [5]. Motivated by these requirements, recent wearable and portable assistive systems have made notable progress through engineering-driven designs. A representative line of work adopts multi-sensor fusion strategies—such as combinations of cameras, active depth sensors, and inertial units—deployed on embedded platforms to close the loop between perception and human feedback. For example, Sight Guide integrates multi-view vision and depth sensing

⋆This work was supported in part by the Fundamental Research Funds for the Central Universities under Grants ZYGX2025YGLH001 and Grant ZYGX2024XJ038, in part by the National Natural Science Foundation of China under Grants 62276055 and 62406062, in part by the Sichuan Science and Technology Program under Grants 2024NSFSC1476 and 2023YFG0288, in part by the Sichuan Provincial Major Science and Technology Project under Grant 2024ZDZX0012.

*Corresponding authors
heqi.eleanore@gmail.com (Q. He); xxwang@uestc.edu.cn (X. Wang); jtzhanguestc@gmail.com (J. Zhang); ybyu@uestc.edu.cn (Y. Yu); hxchu@mail.ustc.edu.cn (H. Chu); fmpfmp@uestc.edu.cn (M. Fan); jycai@uestc.edu.cn (J. Cai); yangzhenglin@cashq.ac.cn (Z. Yang)

with classical robotics pipelines and learning-based components to support obstacle avoidance, object detection, and optical character recognition in real-world tasks [6]. However, survey studies consistently indicate that such sensor-rich and multi-component systems incur substantial overheads in power consumption, wearing comfort, calibration complexity, system cost, and operational robustness, posing significant challenges for sustained daily deployment [7, 8].

Beyond hardware burden, real indoor environments can systematically degrade the reliability of active depth sensing. Transparent or reflective surfaces, narrow passages, and frequent occlusions often result in missing or noisy depth measurements, which may induce unstable or erroneous feedback in safety-critical scenarios [9]. These limitations have motivated growing interest in learning-based 3D environment representations with reduced sensor dependence. In particular, 3D Semantic Scene Completion (SSC) and semantic occupancy prediction aim to recover dense 3D geometry and semantics from limited visual observations, providing structured representations for navigation, interaction, and planning [10]. Under strictly monocular input, MonoScene established a canonical pipeline of 2D feature extraction, 2D-to-3D projection, and volumetric completion, demonstrating the feasibility of monocular SSC from a single RGB image and laying the foundation for subsequent research [11].

Building upon this paradigm, subsequent studies have explored improvements from the perspectives of representation design, global modeling, and computational efficiency. BEVFormer introduced a BEV-centric formulation with Transformer-based aggregation over multi-view and temporal information [12], while TPVFormer further enhanced structural expressiveness through a tri-perspective-view representation [13]. To support scalable training and evaluation, OpenOccupancy and Occ3D constructed larger-scale benchmarks with denser annotations and improved visibility reasoning [14, 15]. Complementarily, SelfOcc explored self-supervised learning from monocular video via rendering consistency, reducing reliance on dense voxel-level annotation [16].

In parallel, increasing attention has been devoted to efficiency, deployability, and effective multi-modal fusion strategies for semantic scene completion. FlashOcc proposed an efficiency-oriented design to balance accuracy and inference speed under practical constraints [17], while OccMamba and MambaOcc leveraged state space models to replace quadratic-complexity global attention for long-range dependency modeling [18, 19]. Beyond architectural efficiency, recent studies have also explored principled fusion mechanisms to better integrate heterogeneous cues. Wang et al. introduced a multi-modal fusion architecture search framework that automatically discovers effective fusion patterns for camera-based semantic scene completion, demonstrating that fusion strategy design plays a critical role in both performance and robustness [20]. For complex indoor environments, ISO and SliceOcc introduced indoor-specialized representations that better align with occlusion patterns and structural layouts [21, 22]. EmbodiedOcc and EmbodiedOcc++ extended occupancy prediction toward embodied online perception via explicit global memory and incremental updates [23, 24]. In camera-based SSC, Bi-SSC and AMMNet improved geometric–semantic consistency through enhanced fusion strategies [25, 26]. Recent generative approaches, such as DiffSSC and GenerativeOcc, further explored diffusion-based priors to hallucinate plausible geometry in heavily occluded regions [27, 28].

Despite these advances, safety-critical visually impaired assistance under monocular or weak-sensor conditions still faces several fundamental challenges. First, the 2D-to-3D lifting process inevitably introduces uncertainty, yet many existing approaches rely on architectural heuristics without explicitly modeling voxel-feature reliability, which is crucial for safety-aware perception [29]. Second, multi-scale feature fusion is often performed via indiscriminate summation or concatenation, potentially propagating projection noise and degrading structural coherence. Third, under deployable constraints such as embedded platforms and limited power budgets, practical improvements cannot rely solely on increasing model capacity, but instead require more robust and reliable feature representations—a trend also reflected in efficiency- and indoor-oriented methods [11, 17, 18, 22, 21, 30].

Motivated by these observations, this work focuses on reliability-oriented modeling and controlled cross-scale information regulation within a monocular SSC framework. By explicitly modeling voxel-feature reliability and stabilizing multi-scale feature fusion, the proposed AMAA framework aims to improve the stability and structural coherence of monocular 3D semantic occupancy prediction while preserving computational efficiency under deployment constraints relevant to safety-critical visually impaired assistive systems.

The main contributions of this work are summarized as follows:

(1) Reliability-oriented formulation for monocular SSC. We revisit the common assumption that lifted voxel features are uniformly reliable after 2D-to-3D projection, and reformulate monocular SSC from the perspective of voxel-feature reliability modeling to improve prediction stability and semantic consistency.

(2) Adaptive multi-scale regulation via joint channel–spatial attention. We propose an adaptive multi-scale feature regulation strategy that jointly models semantic relevance and spatial saliency of voxel representations, mitigating projection-induced diffusion and feature entanglement during multi-scale fusion with limited computational overhead.

(3) Validation under practical deployment constraints. Experiments on the NYU-Depth v2 (NYUv2) benchmark demonstrate that the proposed framework consistently outperforms strong monocular baselines and achieves state-of-the-art performance for single-RGB

semantic scene completion under the standard evaluation protocol.

(4) system-level deployment on an embedded NVIDIA Jetson platform verifies stable end-to-end inference and practical feasibility for safety-critical indoor assistive applications.

The remainder of this paper is organized as follows. Section 2 reviews related work on indoor assistive perception, 3D semantic scene completion and occupancy prediction, monocular and indoor-specific modeling strategies, and efficient edge deployment. Section 3 presents the proposed AMAA framework in detail, including the overall architecture, reliability-oriented voxel feature modeling, parallel channel–spatial attention aggregation, and adaptive multi-scale fusion strategy. Key notations and symbols are summarized in Table 1–2. Section 4 reports experimental results on the NYUv2 benchmark, followed by embedded deployment and runtime validation. Section 5 discusses limitations and failure cases, and Section 6 concludes the paper and outlines future directions.

2. Related Work

2.1. Indoor Assistive Perception and Navigation Systems for Visually Impaired Users

Research on indoor mobility assistance for visually impaired users has long centered on three interrelated goals: reliable perception, safety-critical feedback, and low-burden wearability. Early wearable systems primarily relied on ultrasonic or infrared ranging, which can provide short-range obstacle alerts but lack global structural understanding, limiting their effectiveness in real indoor environments characterized by dense occlusions and layout variability [8].

With advances in embedded computing and visual perception, recent efforts have increasingly shifted toward vision-centric assistive systems. A representative line of work leverages RGB-D sensing, inertial measurements, or multi-sensor fusion to obtain more stable geometric and localization cues, enabling real-time obstacle avoidance and feedback either on-device or at the edge. Many wearable systems integrate RGB-D cameras with inertial modules and classical or learning-based perception pipelines to recognize obstacles and estimate distances, thereby improving independent mobility [6, 31, 32]. Another line emphasizes interactive closed-loop assistance and multi-channel feedback, including speech, haptics, and vibration, with a focus on reducing cognitive load and validating usability in rehabilitation or training scenarios [3, 33].

More recently, lightweight paradigms combining object detection, distance estimation, and high-level scene description or generative prompting have been explored to enhance semantic understanding while maintaining real-time responsiveness [34, 35, 36]. Beyond algorithmic components, body-centric and wearable form factors have been shown to provide more direct and intuitive obstacle cues under daily-life constraints, highlighting the importance of end-to-end system reliability in human-in-the-loop assistance [37]. Complementarily, surveys from the robotics and assistive-navigation communities summarize how SLAM, localization, and mapping pipelines are adapted or constrained in visually impaired assistance, reinforcing that deployable systems must balance sensing burden, compute budget, and robustness in cluttered indoor spaces [38].

Overall, multi-sensor and multi-component systems typically offer advantages in geometric accuracy and robustness, but they also introduce challenges in hardware cost, calibration complexity, power consumption, and long-term wearing comfort. Moreover, active depth sensing can suffer from missing measurements or noise in the presence of transparent or reflective surfaces, narrow passages, and dynamic occlusions, which may compromise the stability of safety-critical feedback. Consequently, obtaining sufficiently reliable 3D environmental representations while reducing dependence on expensive sensors and complex synchronization remains a key challenge for practical assistive perception systems [3, 4, 7].

2.2. 3D Semantic Scene Completion and Semantic Occupancy Prediction

3D Semantic Scene Completion (SSC) and semantic occupancy prediction aim to reconstruct dense 3D occupancy and semantic labels from limited observations, providing a unified representation for navigation, obstacle avoidance, and planning. Recent progress has been driven by advances in representation learning, supervision strategies, and benchmark construction. In camera-based occupancy prediction, BEV representations combined with Transformer-based global modeling have become a dominant paradigm, aggregating multi-view and multi-frame information in BEV space to improve global geometric consistency, as exemplified by BEVFormer [12]. TPVFormer further introduces a tri-perspective-view representation to enhance structural expressiveness for complex 3D scenes [13].

Beyond BEV-style formulations, alternative structured representations and learning objectives have also been explored. OccFormer investigates Transformer architectures tailored to occupancy reasoning, while GaussianFormer employs Gaussian-based representations to compactly model geometry and uncertainty [39, 40]. In parallel, large-scale benchmarks such as OpenOccupancy and Occ3D have promoted more unified training and evaluation protocols, facilitating systematic comparison and accelerating progress in occupancy prediction [14, 15]. To reduce annotation cost, SelfOcc explores self-supervised learning via video consistency and rendering constraints, alleviating reliance on dense voxel-level supervision [16].

Robustness under adverse sensing conditions has also received increasing attention. RadarOcc investigates occupancy prediction using 4D imaging radar, offering an alternative sensing modality for robust perception [41]. Robo3D introduces a comprehensive benchmark to evaluate 3D perception robustness under realistic corruptions, revealing vulnerabilities of existing occupancy models to sensor noise

Table 1
Notation used in the AMAA framework (Part I). All 3D voxel-space tensors follow the channel-first convention unless otherwise specified.

Symbol	Definition
$\mathbf{I} \in \mathbb{R}^{H_I \times W_I \times 3}$	Input RGB image of spatial size $H_I \times W_I$ with three color channels.
$l \in \{1, \dots, L\}$	Feature scale (level) index in the encoder–decoder hierarchy, from higher-resolution shallow levels to lower-resolution deep levels.
$\mathcal{E}(\cdot)$	2D encoder/backbone that extracts multi-scale 2D features from $\mathbf{I}$.
$\mathbf{F}_l^{2D} \in \mathbb{R}^{H_l \times W_l \times C_l}$	2D feature map at scale l with spatial resolution (H_l, W_l) and C_l channels.
$\Phi(\cdot)$ / FLoSP	2D-to-3D lifting operator that projects $\mathbf{F}_l^{2D}$ into a voxel-aligned 3D feature volume using camera geometry and voxel indexing (Fig. 1).
$\mathbf{V}_l \in \mathbb{R}^{C_l \times D_l \times H_l^v \times W_l^v}$	Lifted 3D voxel feature at scale l in channel-first format, with voxel-grid resolution (D_l, H_l^v, W_l^v).
(D, H^v, W^v); (D_l, H_l^v, W_l^v)	Full-resolution voxel grid size and the corresponding scale-l voxel resolution used by multi-scale decoding.
$c \in \{1, \dots, C_l\}$; (d, h, w)	Channel index c and voxel indices (d, h, w) along depth/height/width dimensions.
$\mathbf{z} = [z_1, \dots, z_{C_l}]^\top \in \mathbb{R}^{C_l}$; z_c	Global channel descriptor vector and its c-th element computed by 3D global average pooling in SEBlock-3D (Eq. (4)).
$\mathbf{W}_1, \mathbf{W}_2$	Learnable weights of the bottleneck MLP used in SEBlock-3D for channel recalibration (Eq. (5)).
$\mathbf{s} \in \mathbb{R}^{C_l}$	Channel-wise modulation vector after Sigmoid in SEBlock-3D; broadcast and applied to $\mathbf{V}_l$ (Eq. (6)).
$\mathbf{V}_l^{SE}$	Channel-recalibrated voxel feature produced by SEBlock-3D (Fig. 2).
x_i; μ, σ^2; λ	Scalar voxel activation x_i (at element/voxel index i in $\mathbf{V}_l$), mean μ and variance σ^2 over the SimAM-3D support region, and stabilization constant λ (Eq. (7)).
$e(x_i)$	Energy value assigned by SimAM-3D to activation x_i; higher energy indicates lower relative importance (Eq. (7)).
$\mathbf{A} \in \mathbb{R}^{1 \times D_l \times H_l^v \times W_l^v}$	Voxel-wise spatial attention map produced by SimAM-3D; broadcast across channels when applied to $\mathbf{V}_l$ (Eq. (9), Fig. 3).
$\mathbf{V}_l^{Sim}$	Spatially refined voxel feature after applying SimAM-3D attention (Eq. (9)).

Table 2
Notation used in the AMAA framework (Part II).

Symbol	Definition
$[\cdot;\cdot]$	Channel-wise concatenation operator.
$\odot$	Element-wise (Hadamard) multiplication with broadcasting when required.
$\mathrm{Conv}_{1\times1\times1}(\cdot)$	$1\times1\times1$ 3D convolution used for channel mixing in residual aggregation and gating (Eqs. (10), (11)).
γ	Learnable residual scaling factor initialized to zero for stabilizing residual aggregation (Eq. (10)).
$\mathbf{V}'_l$	Aggregated voxel feature after parallel channel–spatial refinement and residual fusion (Eq. (10)).
$\mathbf{F}_{\mathrm{dec}}^{(l)}$	Decoder feature at stage l after upsampling to voxel resolution (D_l, H_l^v, W_l^v) (Fig. 4).
$\mathbf{M}_l \in [0,1]^{1\times D_l \times H_l^v \times W_l^v}$	Voxel-wise gating map predicted by AFG at stage l, controlling selective encoder-to-decoder injection (Eq. (11)).
α	Scalar coefficient controlling the strength of gated encoder feature injection in AFG (Eq. (12)); selected by ablation (Table 5).
$\mathbf{F}_{\mathrm{fused}}^{(l)}$	Fused decoder feature at stage l after gated residual injection (Eq. (12)).
$\hat{\mathbf{Y}} \in \mathbb{R}^{D\times H^v \times W^v \times C}$	Output voxel-wise semantic class probability tensor on the full-resolution voxel grid.
$\hat{y}_{d,h,w}$	Predicted discrete semantic label for voxel (d, h, w) obtained by $\arg\max$ over classes.
C	Number of semantic classes for SSC, including the empty/free-space class.
$\sigma(\cdot)$; $\delta(\cdot)$	Sigmoid and ReLU activation functions, respectively.
$\mathcal{L}_{\mathrm{total}}, \mathcal{L}_{\mathrm{sem}}, \mathcal{L}_{\mathrm{cons}}$	Total training objective, semantic completion loss, and structural consistency regularizer (Eqs. (13)–(15)).

and environmental perturbations [42]. Efficiency-oriented designs further target practical deployment: ProtoOcc emphasizes accurate and efficient occupancy prediction in unstructured environments, reflecting the growing emphasis on compute-aware 3D reasoning pipelines [43]. In addition, generative approaches such as DiffSSC and Skip-Mamba Diffusion formulate scene completion as a conditional denoising process, leveraging diffusion models to recover plausible geometry in heavily occluded regions, albeit at the cost of increased inference latency [27, 44].

Despite these advances, many SSC and occupancy methods assume richer observations, such as multi-view or multi-frame inputs, which may not align with the sensing and computational constraints of wearable assistive devices. This gap motivates continued interest in monocular or lightweight camera-driven SSC, where prediction stability is as critical as accuracy.

2.3. Monocular and Camera-driven SSC Methods

Under strictly monocular input, MonoScene establishes the canonical "2D feature extraction – 2D-to-3D lifting – voxel-space completion" pipeline, demonstrating the feasibility of predicting SSC from a single RGB image [11]. Subsequent research has primarily focused on improving the quality of lifted voxel features and enhancing the expressiveness and stability of voxel decoding and fusion. For camera-driven SSC, VoxFormer introduces sparse voxel Transformers to better balance representational capacity and computational efficiency during voxel reasoning [45].

Several approaches emphasize joint geometric–semantic modeling. Bi-SSC enhances structural consistency through bidirectional geometry–semantic fusion, while AMMNet improves semantic and geometric representations by more effectively exploiting network capacity [25, 26]. Training-time strategies have also been explored to improve prediction quality without additional inference cost. For example, hardness-aware learning and self-distillation explicitly focus optimization on challenging voxels, addressing the imbalance between dominant empty space and hard boundary regions in dense 3D prediction [46].

Recent studies further address the inherent ambiguity of monocular lifting. Symphonize bridges instance-level and scene-level representations by harmonizing object-centric priors with global scene context [47]. OccNeRF combines neural radiance fields with occupancy prediction, exploiting volume-rendering supervision from monocular sequences to improve geometric fidelity without dense 3D annotations [48]. Vision–language integrated methods such as OccVLM explore open-vocabulary occupancy prediction by leveraging language priors to recognize long-tail objects [49]. Nevertheless, under severe occlusion and pronounced projection uncertainty, noise introduced during 2D-to-3D lifting and multi-scale feature entanglement can still lead to structural instability and semantic discontinuity, which is particularly undesirable for safety-critical assistive feedback.

2.4. Indoor and Embodied Occupancy Modeling

To better capture indoor occlusion patterns, structural diversity, and scale variation, several works propose indoor-specific modeling strategies. ISO focuses on design choices tailored to indoor semantic occupancy prediction to improve robustness under complex occlusions [21]. SliceOcc introduces a vertical-slice representation that better aligns with indoor layouts, achieving strong performance on indoor occupancy benchmarks [22]. Co-Occ further explores multi-modal feature coupling that can gracefully degrade to monocular settings, emphasizing explicit coordination between heterogeneous cues in cluttered environments [50].

In parallel, embodied and online occupancy modeling has gained momentum. EmbodiedOcc extends occupancy prediction to interactive online perception by maintaining an explicit global memory and performing incremental updates, while EmbodiedOcc++ improves update stability with geometric constraints and refined strategies [23, 24]. OccWorld introduces the concept of learning a 3D occupancy world model to predict future scene states [51]. VideoSSC further leverages temporal consistency in monocular video streams to refine static geometric predictions [52]. While these methods address important aspects of real-time and embodied perception, they typically rely on sequential inputs and more complex state maintenance, leaving stability under strictly monocular and resource-constrained settings as an open challenge.

2.5. Edge Deployment and Efficient 3D Perception Inference

Wearable assistive devices require real-time feedback and practical wearability, making deployability and energy efficiency as important as accuracy. Recent edge-AI research emphasizes hardware-aware network design, operator-efficient computation, and end-to-end inference optimization. In 2D dense prediction, hardware-aware lightweight segmentation models illustrate speed–accuracy trade-offs across GPUs and edge devices [53]. From an embedded-systems perspective, TensorRT-oriented acceleration and deployment studies on Jetson-class devices demonstrate that operator choices and runtime optimization substantially affect real-time performance under strict memory and power budgets [54, 55].

For 3D occupancy and SSC, efficiency-oriented pipelines explicitly target embedded inference. FlashOcc balances accuracy and throughput via efficiency-driven design [17]. A notable emerging trend is the application of State Space Models (SSMs) to 3D perception. MambaOcc and OccMamba leverage selective scan mechanisms to model long-range 3D dependencies with linear complexity [18, 19]. Additional efforts, such as LightOcc, emphasize lightweight spatial priors and deployability-oriented designs [56]. Hydra demonstrates an asynchronous edge-based 3D perception framework [30], and LMPOcc explores sparse convolution kernels optimized for mobile GPUs [57]. Collectively, these studies indicate that improving 3D perception under resource constraints often requires hardware-friendly feature

construction and information-flow regulation rather than increasing model complexity.

2.6. Summary

In summary, substantial progress has been achieved across assistive-system engineering, 3D perception representations, semantic scene completion and occupancy supervision, indoor- and embodied-aware modeling, as well as efficient edge inference. Despite these advances, under the combined constraints of strictly monocular input and limited on-device computational resources, fundamental challenges remain. In particular, uncertainty introduced during the 2D-to-3D lifting process and the uncontrolled propagation of unreliable features through conventional multi-scale fusion can significantly undermine structural stability and semantic consistency. Such instability is especially critical for safety-related indoor assistive applications, where unreliable or fragmented 3D predictions may directly affect downstream warning and guidance behaviors. These observations motivate a reliability-aware formulation of monocular indoor SSC, emphasizing explicit regulation of voxel feature trustworthiness and controlled cross-scale information flow within a deployable framework, rather than relying solely on increased model capacity or additional sensing modalities.

3. Methods

3.1. Overview and Motivation

This paper focuses on monocular 3D semantic scene completion (SSC) for indoor assistive perception targeting visually impaired users. In safety-critical indoor mobility, the perception module must provide not only object categories but also a stable and structurally consistent 3D understanding of free space and obstacles, so that real-time warnings remain reliable in cluttered environments. Compared with sensor-rich solutions (e.g., RGB-D/LiDAR), monocular SSC is attractive for wearable assistive devices due to its lower hardware cost, reduced calibration burden, and better portability under power/compute constraints.

Recent MonoScene-style pipelines have established an efficient "2D encoding → 2D-to-3D lifting → 3D completion" paradigm, demonstrating that a single RGB image can be lifted to voxel space and decoded into dense semantic occupancy. We acknowledge the contribution of this paradigm as it enables sensor-efficient 3D perception and practical deployment. However, strict monocular lifting inevitably introduces projection uncertainty (occlusion, depth ambiguity, textureless/reflective surfaces), yielding uneven reliability across lifted voxel features. Moreover, conventional multi-scale decoding often injects encoder features through skip connections indiscriminately, which may propagate projection noise and cause fragmented structures (e.g., isolated "floating" voxels). Such artifacts are particularly undesirable for visually impaired assistive systems, where unstable predictions may lead to delayed or incorrect feedback.

To address these limitations, this paper propose the Adaptive Multi-scale Attention Aggregation Framework (AMAA) (Fig. 1). AMAA retains the original monocular SSC backbone while introducing two reliability-aware designs: (i) a parallel channel–spatial attention aggregation module operating on 3D voxel features (Figs. 2–3) to explicitly regulate feature reliability after lifting, and (ii) a hierarchical Adaptive Feature Gating (AFG) mechanism (Fig. 4) to selectively fuse multi-scale information during decoding. The overall principle is to regulate information flow based on reliability, rather than increasing model capacity, which is beneficial for edge deployment and stable assistive perception.

3.2. Problem Formulation

Given an RGB image $\mathbf{I} \in \mathbb{R}^{H_I \times W_I \times 3}$, the goal is to predict voxel-wise semantic occupancy over a 3D grid. Let $\hat{\mathbf{Y}} \in \mathbb{R}^{D \times H^v \times W^v \times C}$ denote the predicted voxel-wise semantic probability distribution, where D, H^v, W^v are the voxel grid dimensions and C is the number of semantic classes (including empty). For each voxel index (d, h, w), the predicted label is

$$\hat{y}_{d,h,w} = \arg \max_{c \in \{1,\dots,C\}} \hat{\mathbf{Y}}(d, h, w, c). \tag{1}$$

3.3. Monocular SSC Backbone and Its Limitations

Following the MonoScene-style pipeline (Fig. 1), a 2D encoder extracts multi-scale 2D features:

$$\{\mathbf{F}_l^{2D}\}_{l=1}^{L} = \mathcal{E}(\mathbf{I}), \tag{2}$$

where $\mathcal{E}(\cdot)$ denotes the 2D backbone and $\mathbf{F}_l^{2D} \in \mathbb{R}^{H_l \times W_l \times C_l}$ is the feature map at scale l.

Then, a lifting operator $\Phi(\cdot)$ (FLoSP in Fig. 1) projects 2D features into a 3D voxel space:

$$\mathbf{V}_l = \Phi(\mathbf{F}_l^{2D}), \qquad \mathbf{V}_l \in \mathbb{R}^{C_l \times D_l \times H_l^v \times W_l^v}. \tag{3}$$

While this backbone is efficient and deployment-friendly, it implicitly treats lifted voxel features as equally reliable. In real indoor scenes, projection uncertainty leads to spatially varying noise and ambiguous cues; if such unreliable signals are propagated via indiscriminate multi-scale fusion, the decoder may amplify artifacts and produce structurally inconsistent occupancy. This instability directly undermines the reliability required by visually impaired assistive systems. AMAA explicitly addresses this issue by regulating 3D voxel feature reliability after lifting and controlling cross-scale information injection during decoding.

3.4. Parallel Channel–Spatial Attention Aggregation on 3D Voxel Features

As shown in Fig. 1, AMAA refines each lifted 3D feature $\mathbf{V}_l$ using a parallel channel–spatial aggregation module composed of SEBlock-3D (Fig. 2) and SimAM-3D (Fig. 3). Importantly, both mechanisms operate on 3D voxel features with shape $C_l \times D_l \times H_l^v \times W_l^v$, consistent with the feature dimensions illustrated in the figures.

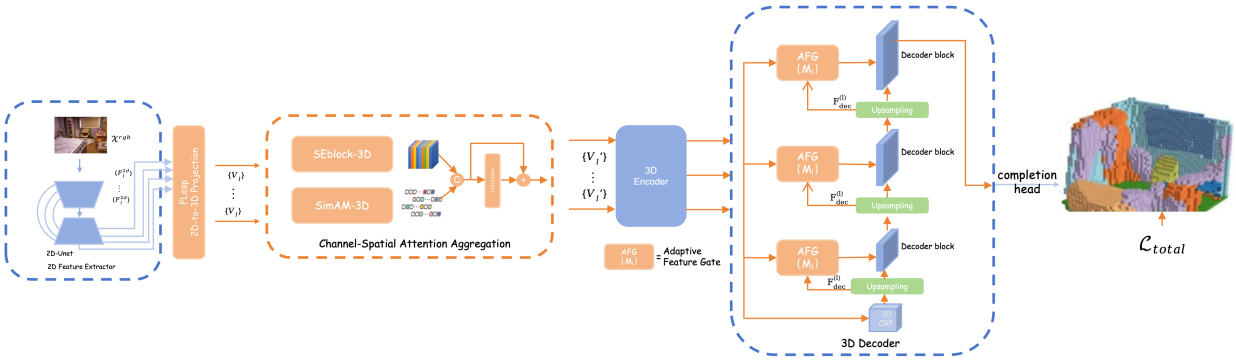

Fig. 1: Overall architecture of the proposed AMAA framework. Multi-scale 2D features extracted from the input RGB image are lifted into a 3D voxel space via the FLoSP projection operator. The lifted voxel features are refined by a parallel channel–spatial aggregation module (SEBlock-3D and SimAM-3D), followed by a 3D decoder equipped with Adaptive Feature Gating (AFG) blocks for regulated multi-scale fusion, producing voxel-wise semantic occupancy predictions over the 3D voxel grid.

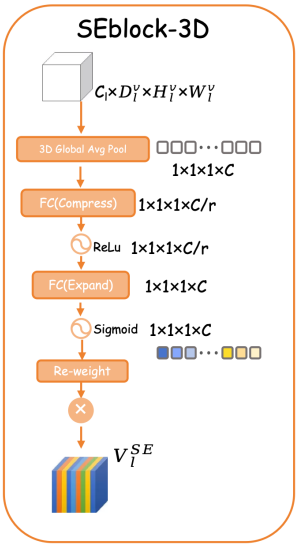

Fig. 2: SEBlock-3D for channel-wise recalibration in voxel space. The module applies global 3D average pooling to summarize channel responses and uses a lightweight bottleneck MLP to generate channel-wise modulation weights, enhancing informative semantic channels in volumetric features.

3.4.1. *Channel-wise semantic recalibration via SEBlock-3D*

SEBlock-3D models inter-channel dependencies to emphasize semantically informative channels (Fig. 2). this paper first compute a global descriptor by 3D global average pooling:

$$z_c = \frac{1}{D_l H_l^v W_l^v} \sum_{d=1}^{D_l} \sum_{h=1}^{H_l^v} \sum_{w=1}^{W_l^v} \mathbf{V}_l(c,d,h,w), \tag{4}$$

where z_c is the aggregated response of channel c and $\mathbf{V}_l(c,d,h,w)$ denotes the scalar activation at voxel (d,h,w) in channel c.

A lightweight bottleneck MLP then produces channel modulation weights:

$$\mathbf{s} = \sigma\big(\mathbf{W}_2\,\delta(\mathbf{W}_1\mathbf{z})\big), \qquad \mathbf{z} = [z_1,\ldots,z_{C_l}]^\top \in \mathbb{R}^{C_l}, \tag{5}$$

where $\mathbf{W}_1, \mathbf{W}_2$ are learnable parameters, $\delta(\cdot)$ is ReLU, and $\sigma(\cdot)$ is Sigmoid. The channel-recalibrated feature is

$$\mathbf{V}_l^{SE} = \mathbf{s} \odot \mathbf{V}_l, \tag{6}$$

where $\odot$ denotes channel-wise multiplication with broadcasting over (D_l, H_l^v, W_l^v).

After lifting, different channels contribute unequally to robust 3D semantics in cluttered indoor scenes. SEBlock-3D strengthens semantically relevant channels while suppressing noisy responses, thereby improving semantic consistency in voxel representations and stabilizing assistive perception outputs.

3.4.2. *Parameter-free spatial refinement via SimAM-3D*

To enhance geometry awareness without increasing model capacity, this paper adopt a parameter-free SimAM mechanism in 3D voxel space (Fig. 3). For each voxel activation x_i (a scalar activation at voxel index i in $\mathbf{V}_l$), this paper compute an energy function using local 3D neighborhood statistics:

$$e(x_i) = \frac{(x_i-\mu)^2}{4(\sigma^2+\lambda)} + 0.5, \tag{7}$$

where μ and σ^2 are the mean and variance of activations in a local 3D neighborhood (e.g., $3\times3\times3$) centered at x_i, and λ is a small stabilization constant for numerical robustness.

The voxel-wise spatial attention map is derived as:

$$\mathbf{A} = \sigma\left(\frac{1}{e(x_i)}\right), \tag{8}$$

where $\mathbf{A} \in \mathbb{R}^{1\times D_l\times H_l^v\times W_l^v}$ (broadcastable to channels). The spatially refined feature is

$$\mathbf{V}_l^{Sim} = \mathbf{V}_l \odot \mathbf{A}. \tag{9}$$

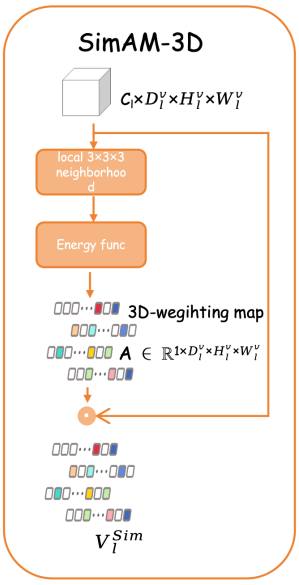

Fig. 3: SimAM-3D for parameter-free spatial reweighting in voxel space. The module computes an energy-based importance score for each voxel activation using region-wise activation statistics, producing a spatial attention map without introducing additional learnable parameters.

Unreliable voxels (often caused by occlusion and depth ambiguity) tend to exhibit higher energy and are down-weighted. This suppresses projection artifacts and improves structural stability, which is crucial for safety-critical warnings in visually impaired indoor navigation.

3.4.3. Residual feature aggregation

This paper fuse the two branches using a residual formulation (consistent with Fig. 1):

$$\mathbf{V}'_l = \mathbf{V}_l + \gamma \cdot \mathrm{Conv}_{1\times1\times1}\left([\mathbf{V}_l^{SE}; \mathbf{V}_l^{Sim}]\right), \tag{10}$$

where $[\cdot;\cdot]$ denotes channel concatenation, $\mathrm{Conv}_{1\times1\times1}$ is a $1 \times 1 \times 1$ 3D convolution for feature mixing, and γ is a learnable scaling factor initialized to zero to stabilize early optimization. The refined features $\{\mathbf{V}'_l\}$ are fed to the 3D encoder and then the 3D decoder (Fig. 1).

3.5. Hierarchical Adaptive Multi-scale Fusion with AFG

Multi-scale fusion is essential for balancing global semantic coherence and local geometric precision in monocular SSC. Fine-resolution encoder features preserve high-frequency details, yet they are also more sensitive to projection uncertainty and may carry noisy lifted signals. In contrast, decoder features tend to be more stable but can be over-smoothed, leading to blurred boundaries. Conventional skip connections typically fuse multi-scale features uniformly (e.g., concatenation or summation), which may indiscriminately propagate unreliable high-resolution cues and cause fragmented reconstructions (e.g., isolated "floating" voxels). Such instability is particularly undesirable for visually impaired assistive navigation, where unreliable 3D occupancy predictions can trigger incorrect warnings or delayed feedback.

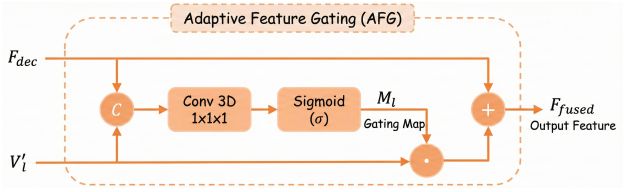

Fig. 4: Adaptive Feature Gating (AFG) module for regulated multi-scale fusion. AFG predicts a voxel-wise gating map conditioned on decoder and encoder features, enabling selective injection of fine-scale encoder information into the decoder through gated residual fusion.

To address this issue, this paper introduce a Hierarchical Adaptive Feature Gating (AFG) mechanism (Fig. 4) that selectively regulates encoder-to-decoder information flow at each decoding stage. Specifically, at decoding stage l, given an upsampled decoder feature $\mathbf{F}_{\mathrm{dec}}^{(l)} \in \mathbb{R}^{C_d \times D_l \times H_l^v \times W_l^v}$ and the corresponding refined encoder feature $\mathbf{V}'_l \in \mathbb{R}^{C_e \times D_l \times H_l^v \times W_l^v}$, this paper first compute a voxel-wise gating map:

$$\mathbf{M}_l = \sigma\Big(\mathrm{Conv}_{1\times1\times1}\left([\mathbf{F}_{\mathrm{dec}}^{(l)}; \mathbf{V}'_l]\right)\Big), \tag{11}$$

where $[\cdot;\cdot]$ denotes channel-wise concatenation, $\mathrm{Conv}_{1\times1\times1}$ is a $1\times1\times1$ 3D convolution, and $\sigma(\cdot)$ is the Sigmoid function. The gating map $\mathbf{M}_l \in [0,1]^{1\times D_l \times H_l^v \times W_l^v}$ encodes the spatial confidence of injecting encoder cues into the decoder at scale l.

This paper then perform gated residual fusion with a scaling coefficient α:

$$\mathbf{F}_{\mathrm{fused}}^{(l)} = \mathbf{F}_{\mathrm{dec}}^{(l)} + \alpha\left(\mathbf{M}_l \odot \mathbf{V}'_l\right), \tag{12}$$

where $\odot$ denotes element-wise multiplication (broadcasted to channels when needed), and $\alpha \in \mathbb{R}^+$ controls the injection strength of gated encoder features. In particular, $\alpha = 0$ degenerates to removing the gated injection branch, while larger α injects more high-frequency cues.

$\mathbf{F}_{\mathrm{dec}}^{(l)}$ provides a stable global semantic backbone, whereas $\mathbf{V}'_l$ contributes fine-grained details that are useful but potentially noisy under monocular projection. The gating map $\mathbf{M}_l$ suppresses unreliable voxel regions and permits feature injection only where the fused evidence is confident. The additional coefficient α further calibrates the overall contribution of gated encoder cues, allowing a principled trade-off between detail preservation and noise amplification. Applying AFG hierarchically across decoding stages (Fig. 1) progressively refines scene structure from coarse to fine, improving structural consistency and stabilizing occupancy predictions in cluttered indoor scenes, which is crucial for safety-critical assistive perception for visually impaired users.

Effect of the AFG scaling coefficient. This paper ablate the scaling coefficient α in Eq. (12) to quantify how the

injection strength affects performance. As summarized in Table 5, setting $\alpha = 0$ (removing gated injection) yields a clear performance drop, confirming the benefit of selectively injecting encoder cues. Increasing α improves performance up to an optimal value, after which overly strong injection may amplify projection-induced noise. Unless otherwise specified, this paper set $\alpha = 0.75$ (the best value in Table 5) in all experiments.

3.6. Loss Function

To jointly optimize semantic accuracy and structural coherence, the total training objective is defined as:

$$\mathcal{L}_{\text{total}} = \mathcal{L}_{\text{sem}} + \lambda_c \mathcal{L}_{\text{cons}}, \tag{13}$$

where $\mathcal{L}_{\text{sem}}$ is the semantic completion loss, $\mathcal{L}_{\text{cons}}$ is a structural consistency regularizer, and λ_c balances the two terms.

This paper adopt a weighted cross-entropy loss to address class imbalance and complement it with a geo-semantic affinity term:

$$\mathcal{L}_{\text{sem}} = \mathcal{L}_{ce} + \mathcal{L}_{\text{geo-sem}}, \tag{14}$$

where $\mathcal{L}_{ce}$ is voxel-wise weighted cross-entropy and $\mathcal{L}_{\text{geo-sem}}$ is the geo-semantic affinity loss term as defined in the baseline setting.

To suppress isolated predictions and encourage local geometric continuity, this paper introduce a neighborhood consistency term:

$$\mathcal{L}_{\text{cons}} = \sum_i \left| \hat{Y}_i - \text{AvgPool}(\hat{Y})_{\mathcal{N}(i)} \right|, \tag{15}$$

where i indexes voxels, $\hat{Y}_i$ denotes the predicted occupancy/semantic response at voxel i (e.g., a probability score), $\mathcal{N}(i)$ is a local voxel neighborhood around i, and $\text{AvgPool}(\cdot)_{\mathcal{N}(i)}$ computes neighborhood average pooling. This term promotes locally coherent occupancy patterns and reduces spurious "floating" voxels, improving reliability in safety-critical assistive navigation.

3.7. Discussion: Relevance to Visually Impaired Assistive Perception

AMAA maintains a sensor-efficient monocular pipeline and targets the key bottleneck for assistive indoor perception: instability caused by projection uncertainty and indiscriminate multi-scale fusion. The proposed channel–spatial aggregation explicitly regulates voxel feature reliability after lifting (Figs. 2–3), while AFG prevents noisy high-resolution signals from being injected everywhere (Fig. 4). These reliability-aware mechanisms improve structural consistency without significantly increasing computational overhead, making AMAA suitable as a core perception module for visually impaired indoor assistive devices deployed on resource-constrained edge platforms (e.g., Jetson), where stable real-time feedback is required.

4. Experiment

This section evaluates the proposed AMAA framework under the standard indoor Semantic Scene Completion (SSC) protocol and analyzes its practical relevance to safety-critical assistive perception for visually impaired users. In indoor navigation assistance, a perception framework is required not only to achieve high average accuracy on benchmarks, but also to provide stable, structurally consistent, and interpretable 3D semantic occupancy under frequent occlusions, severe scale variation, and incomplete visual evidence. Monocular SSC is particularly challenging in this regard, as the 2D-to-3D lifting process is inherently ambiguous and may introduce uneven voxel-feature reliability and projection-induced noise that accumulates during multi-scale decoding.The AMAA framework addresses these challenges from a system-design perspective by (i) explicitly regulating the reliability of lifted 3D voxel representations through joint semantic–geometric attention aggregation, and (ii) performing hierarchical adaptive multi-scale fusion via gated information injection, which selectively propagates encoder cues to the decoder. This paper validate these design principles through quantitative comparisons, ablation studies, and qualitative analyses, while preserving the original experimental figures and tables in this manuscript.

4.1. Dataset and Evaluation Protocol

Dataset. This paper conduct experiments on NYU-Depth v2 (NYUv2), a widely adopted indoor benchmark that contains diverse cluttered scenes such as homes, offices, and classrooms, with dense semantic annotations [58]. The dataset exhibits frequent occlusions, narrow passages, and heterogeneous object layouts, which resemble real indoor environments encountered by visually impaired users and are therefore suitable for evaluating robustness-oriented SSC frameworks.

Monocular setting. Following the common monocular SSC protocol [59, 11], the proposed framework operates strictly on a single RGB image at inference time. Depth information is used only during training to construct voxel-level semantic supervision following the standard SSC label generation pipeline [59]. This setting ensures a fair and controlled comparison with prior monocular SSC approaches and isolates the contribution of the proposed framework-level designs.

Voxelization. The camera frustum is discretized into a fixed voxel grid, and the framework predicts both occupancy and semantic labels for each voxel. This voxel-based representation aligns naturally with downstream navigation and obstacle-awareness tasks and is also compatible with deployment constraints on wearable or embedded platforms.

Evaluation metrics. This paper report two standard SSC metrics [59]: (i) Scene Completion IoU (SC IoU) for binary occupancy prediction, and (ii) Semantic Scene Completion mean IoU (SSC mIoU) over semantic classes (excluding empty) as the primary semantic metric. For the sensitivity analysis of gated feature injection, this paper additionally report Precision and Recall to characterize the trade-off

between conservative and aggressive occupancy prediction under monocular uncertainty.

4.2. Implementation Details

The AMAA framework is implemented on top of a MonoScene-style monocular SSC pipeline (Fig. 1) [11]. To ensure controlled evaluation, this paper follow the standard training protocol commonly adopted in prior monocular SSC studies and introduce the proposed reliability-oriented designs only at two stages: (i) regulation of lifted 3D voxel features after 2D-to-3D projection, and (ii) hierarchical adaptive multi-scale fusion during decoding. The underlying backbone architecture and training recipe remain unchanged unless explicitly stated.

Unless otherwise specified, the gated injection scaling coefficient is fixed to $\alpha = 0.75$, which achieves the best overall performance in Table 5. All experiments are conducted on a workstation equipped with two NVIDIA GeForce RTX 4090 GPUs. The framework is implemented in PyTorch with CUDA acceleration, and all baseline methods and ablation variants are trained and evaluated under the same hardware and software environment for fair comparison.

Following the common NYUv2 SSC protocol [58, 59, 11], each RGB image is resized to 480×640 and normalized using ImageNet statistics. Depth maps are used only during training to generate voxel-level supervision, while inference strictly operates on monocular RGB input. Standard data augmentation, including random horizontal flipping, mild color jittering, and random scaling and cropping, is applied during training to improve generalization across diverse indoor layouts.

The 3D space is discretized into a voxel grid of size $60 \times 36 \times 60$ with a voxel resolution of 0.08 m, which offers a practical balance between geometric fidelity and computational cost and is consistent with widely used SSC configurations [59, 11]. The framework is optimized using AdamW with an initial learning rate of 1×10^{-4} and a weight decay of 1×10^{-2}. A polynomial learning-rate decay schedule is adopted, and the framework is trained for 30 epochs with a total batch size of 2 (1 image per GPU). Mixed-precision training is used to reduce memory footprint and accelerate optimization.

4.3. Comparison with Prior Methods

Table 3 reports quantitative results on NYUv2 under the monocular SSC setting. AMAA achieves the best overall performance among the compared methods, reaching an SC IoU of 43.10% and an SSC mIoU of 27.25%. Compared with the monocular baseline MonoScene [11], AMAA improves SC IoU from 42.51% to 43.10% and increases SSC mIoU from 26.94% to 27.25%, demonstrating consistent gains in both geometric completion and semantic occupancy prediction without relying on additional sensors. AMAA also maintains clear margins over earlier SSC baselines (e.g., LMSCNet, AIC-Net, and 3DSketch), indicating its effectiveness across diverse indoor layouts.

Beyond the overall averages, Fig. 5 provides a category-wise view by summarizing the distribution of SSC IoU scores across semantic categories. The boxplots show that AMAA generally yields higher median IoUs across most categories, spanning both structural classes (e.g., ceiling, floor, wall) and common indoor objects/furniture (e.g., chair, bed, sofa, table, furniture, and miscellaneous objects). This trend suggests that AMAA improves not only mean performance but also the robustness of semantic completion across heterogeneous scene components, which is particularly important in cluttered indoor environments where monocular lifting uncertainty varies spatially and semantically.

Fig. 6 further complements the quantitative comparison from two perspectives. First, the category-level visualization heatmap highlights that the improvements are not concentrated in a single class but are distributed across multiple indoor categories, supporting the claim that the proposed reliability-oriented formulation provides broadly applicable benefits rather than class-specific tuning. Second, the training curves in Fig. 6 indicate stable optimization behavior, showing that introducing reliability regulation and hierarchical adaptive fusion does not compromise convergence and can be trained consistently under the standard monocular SSC recipe. From an assistive navigation perspective, these results imply more reliable and structurally coherent 3D semantic occupancy for downstream warning and guidance. In particular, improving category-level robustness (Fig. 5) while maintaining stable training dynamics (Fig. 6) helps mitigate unstable voxel predictions that may otherwise translate into inconsistent obstacle signals, thereby supporting safer indoor mobility assistance for visually impaired users.

4.4. Ablation Studies

This paper perform ablations to validate the contribution of each proposed design and to clarify how the method alleviates monocular uncertainty, especially in cluttered indoor scenes relevant to visually impaired assistance.

4.4.1. Incremental Effect of Reliability Regulation and Hierarchical Adaptive Fusion

Table 4 (original table in this paper) reports the incremental results (A/B/C/D) when introducing reliability regulation and hierarchical adaptive fusion. The consistent improvement across SC IoU and SSC mIoU supports our central claim: in monocular SSC, performance is limited not only by missing information but also by unreliable lifted 3D cues and indiscriminate cross-scale propagation. By regulating voxel-feature reliability and selectively injecting encoder cues into the decoder, AMAA improves both semantic coherence and geometric consistency without relying on additional sensors.

4.4.2. Sensitivity to the Gated Injection Strength

As described in Sec. 3.5 Eq. (12), hierarchical adaptive fusion adopts gated residual injection. where α controls the overall injection strength of gated encoder cues. This coefficient is practically important: too small α under-utilizes informative high-resolution cues, whereas too large α may amplify projection-induced noise even with gating.

Table 3
Quantitative comparison on semantic scene completion (SSC) on NYUv2 dataset. The proposed AMAA-Framework yields higher overall mIoU than the baseline MonoScene.

Method	Input	SC	SSC											mIoU(%)
		IoU	ceil.	floor	wall	win.	chair	bed	sofa	table	tvs	furn.	objs.	
LMSCNet [60]	C	33.93	4.49	88.41	4.63	0.25	3.94	32.03	15.44	6.57	0.02	14.51	4.39	15.88
AICNet [61]	C&L	30.03	7.58	82.97	9.15	0.05	6.93	35.87	22.92	11.11	0.71	15.90	6.45	18.15
3DSketch [62]	C&D	38.64	8.53	90.45	9.94	5.67	10.64	42.29	29.21	13.88	9.38	23.83	8.19	22.91
MonoScene [11]	C	42.51	8.89	93.50	12.06	12.57	**13.72**	48.19	36.11	15.13	15.22	27.96	12.94	26.94
AMAA(Ours)	C	**43.10**	**9.33**	**93.55**	**12.07**	**13.12**	13.64	**49.80**	**36.24**	**15.60**	**16.15**	**28.10**	**13.75**	**27.25**

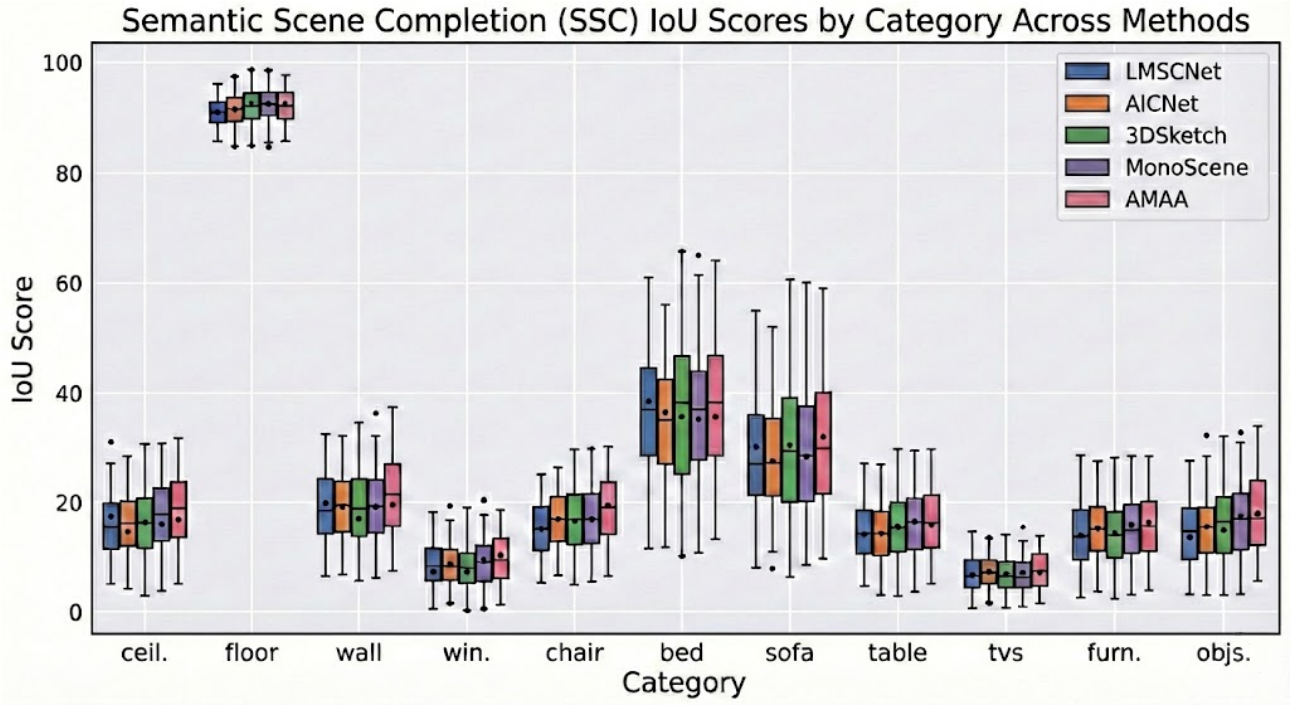

Fig. 5: Category-wise SSC IoU distributions on NYUv2 across methods. The boxplots summarize per-category IoU scores (median, interquartile range, and whiskers) for LMSCNet, AICNet, 3DSketch, MonoScene, and the proposed AMAA. Overall, AMAA exhibits consistently higher medians across most semantic categories, indicating more reliable semantic occupancy completion under monocular constraints.

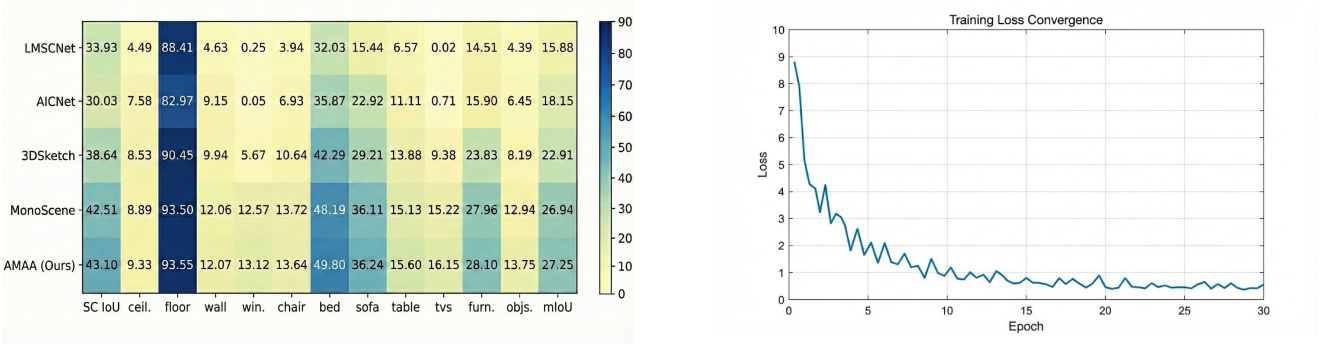

Fig. 6: Visualization of experimental analysis. **(Left)** Heatmap comparison of IoU performance on the NYUv2 dataset. Darker colors indicate higher scores, highlighting that our AMAA-Framework achieves superior results across most categories. **(Right)** Training loss convergence curve, demonstrating the stable learning process of our Framework over 30 epochs.

Table 4
Ablation study on the NYUv2 test set. SE: SEBlock-3D Channel Attention; Sim: SimAM-3D Spatial Attention; AFG: Adaptive Feature Gating.

Model	SE	Sim	AFG	SC IoU	mIoU(%)
A (Baseline)				42.51	26.94
B	✓			42.75	27.08
C	✓	✓		42.92	27.16
D (Ours)	✓	✓	✓	**43.10**	**27.25**

Table 5
Ablation on the scaling coefficient α in AFG (Eq. (12)). α controls the injection strength of gated encoder features.

α	mIoU(%)	IoU	Precision	Recall
0.00	25.80	41.20	55.05	64.30
0.25	26.45	42.51	56.14	65.12
0.50	27.07	42.84	56.43	65.71
0.75	27.25	43.10	56.85	66.21
1.00	27.13	42.87	56.32	65.94
1.25	26.85	42.53	55.71	65.13
Best (0.75)	**27.25**	**43.10**	**56.85**	**66.21**

Table 5 shows that removing gated injection ($\alpha = 0$) significantly degrades performance (mIoU drops from 27.25% to 25.80%; IoU drops from 43.10% to 41.20%), confirming the necessity of selectively propagating encoder cues in monocular SSC. Increasing α improves all metrics up to $\alpha = 0.75$, which achieves the best overall results (mIoU 27.25%, IoU 43.10%, Precision 56.85%, Recall 66.21%). Further increasing α leads to a slight decline (e.g., mIoU 27.13% at $\alpha = 1.0$ and 26.85% at $\alpha = 1.25$), suggesting that overly strong injection may re-introduce noise through the multi-scale pathway. Therefore, this paper set $\alpha = 0.75$ as the default configuration in all experiments.

4.5. Embedded Deployment and Real-world Inference Validation

To evaluate the practical deployability of the proposed AMAA framework, this paper conducts a system-level *inference-only* deployment study on an NVIDIA Jetson Orin NX platform. Unlike benchmark-style evaluations that primarily emphasize inference speed or parameter efficiency, this study aims to verify that a *pretrained* monocular SSC framework can be executed end-to-end on embedded hardware and can produce stable and interpretable 3D semantic occupancy predictions from real-world visual inputs under realistic operating conditions.

Deployment setup. The AMAA framework is deployed on an NVIDIA Jetson Orin NX device using the *same pretrained network weights* obtained from the offline NYUv2 benchmark experiments. No retraining, fine-tuning, or adaptation is performed on the embedded device. Inference is conducted under a strictly monocular setting, where a single RGB image serves as the sole input. All components of the framework—including 2D feature extraction, 2D-to-3D voxel lifting, reliability-oriented voxel feature regulation via channel–spatial attention, and hierarchical adaptive multi-scale fusion—are executed end-to-end during forward inference on the embedded platform.

To reflect a realistic deployment scenario, no model compression, parameter pruning, quantization, or hardware-specific optimization is applied. This setup allows us to isolate and evaluate the intrinsic deployability of the proposed framework design without confounding effects from additional engineering optimizations.Fig. 9 illustrates the embedded inference setup used in our real-world experiments. The system integrates a Jetson Orin NX module as the embedded computing unit, a ZED 2i camera operated in monocular RGB mode during inference, and an external portable power supply, forming a fully self-contained platform suitable for indoor assistive perception validation.

Real-world inference validation. To assess generalization beyond curated benchmarks, we perform inference on real-world indoor images captured by the authors using a handheld RGB camera. These images depict everyday indoor environments with cluttered furniture layouts, varying illumination conditions, and partial occlusions representative of scenarios encountered in practical assistive navigation. Representative qualitative results are shown in Fig. 8, where the AMAA framework generates 3D semantic occupancy predictions directly from single RGB inputs using the pretrained model.

Observations and discussion. Qualitative inspection of the real-world inference results indicates that the AMAA framework preserves coherent structural layouts and continuous free-space regions, while avoiding excessive fragmentation or unstable responses. In challenging areas with reflective surfaces or weak texture, failure cases tend to manifest as conservative completion rather than aggressive hallucination. Such behavior is generally preferable for safety-critical visually impaired assistance, where unstable or oscillatory predictions may lead to misleading feedback. These observations are consistent with the qualitative trends observed in the NYUv2 benchmark (Fig. 7) and further support the reliability-oriented design philosophy underlying the proposed framework.

Overall, this deployment study demonstrates that the proposed AMAA framework, trained offline and deployed without modification, can be executed reliably on embedded hardware and can generalize to real-world monocular visual inputs. While no quantitative runtime or parameter comparisons are performed, the results provide practical evidence of feasibility for inference-only deployment of monocular semantic scene completion frameworks in resource-constrained visually impaired assistive systems.

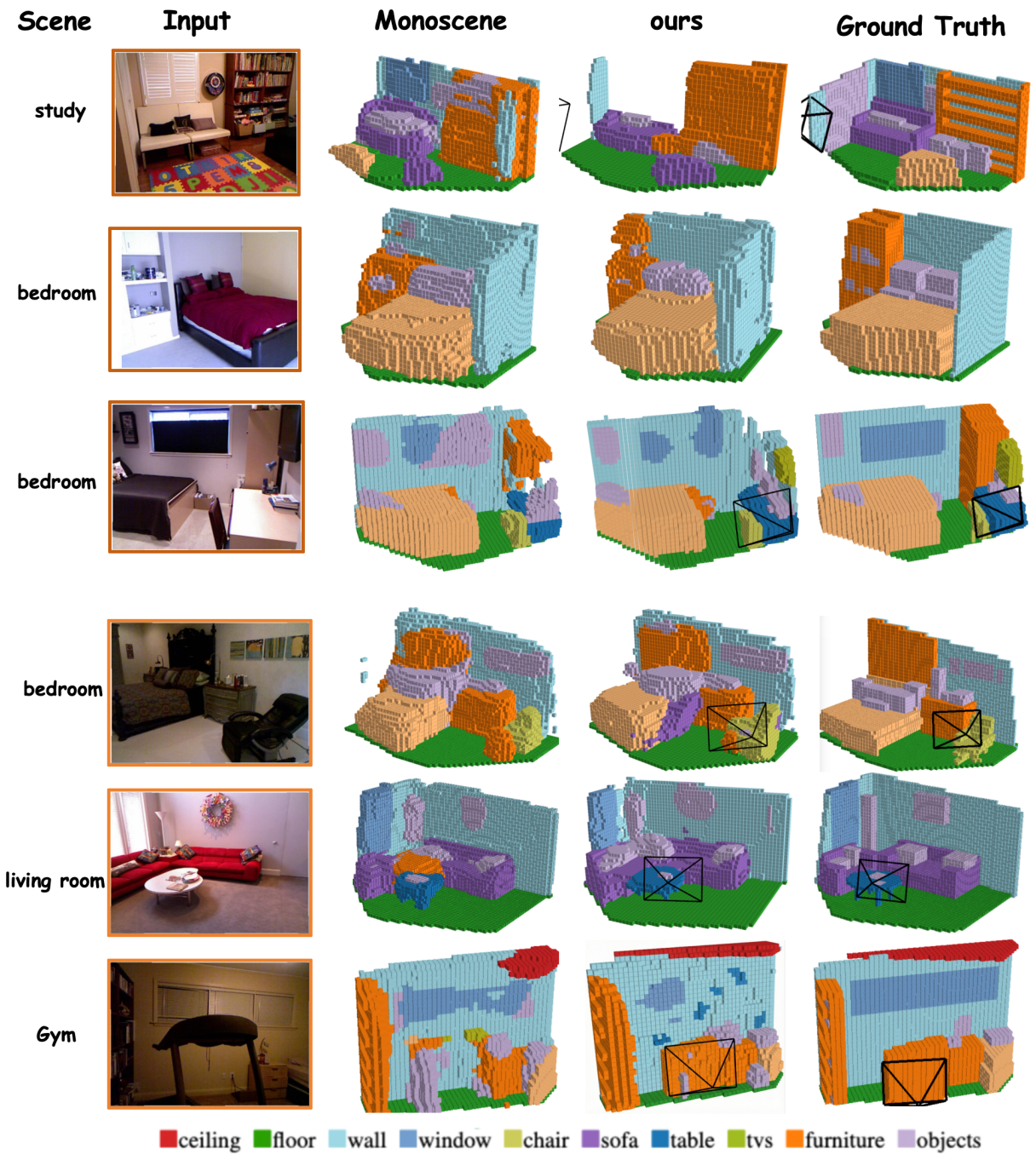

Fig. 7: Qualitative results on NYUv2. From left to right: Input RGB, Ground Truth, MonoScene, and Ours (AMAA). Red boxes highlight regions where the proposed framework recovers finer structural details compared to the baseline.

5. Discussion and Failure Cases

While the proposed AMAA framework consistently improves monocular SSC performance, several limitations remain that are intrinsic to monocular 3D semantic scene completion. Discussing these cases is important for clarifying the scope of applicability of AMAA in safety-critical indoor assistive perception, particularly under realistic deployment conditions.

Ambiguity in textureless and reflective regions. Indoor regions dominated by textureless surfaces (e.g., plain walls) or reflective and transparent materials (e.g., mirrors and glass) provide inherently weak monocular constraints on depth ordering. In such cases, the 2D-to-3D lifting process may yield spatially diffused voxel activations along viewing rays, leading to locally over-smoothed or uncertain occupancy predictions. Although AMAA explicitly regulates

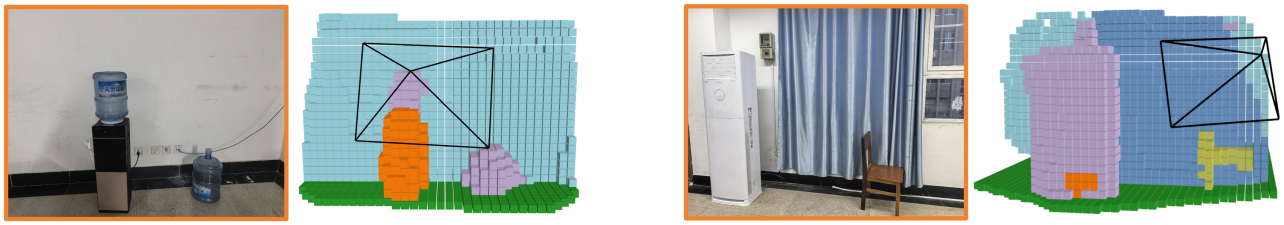

Fig. 8: Qualitative results of monocular 3D semantic scene completion on real-world indoor images. From left to right, each example shows the input RGB image and the corresponding 3D semantic occupancy prediction generated by the proposed method.

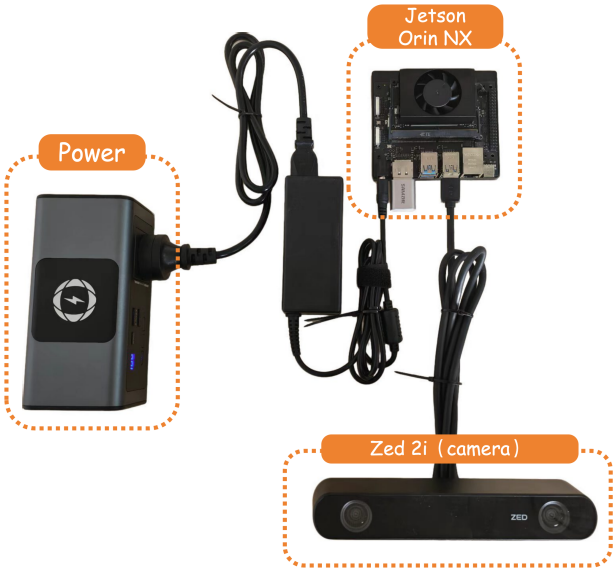

Fig. 9: Embedded deployment setup of the proposed AMAA framework on an NVIDIA Jetson Orin NX platform. The system consists of a Jetson Orin NX embedded computing unit, a ZED 2i camera used in monocular RGB mode during inference, and an external portable power supply. All components are connected and operated in a self-contained configuration for real-world indoor semantic scene completion.

voxel-feature reliability via channel–spatial aggregation, extremely ambiguous visual evidence remains difficult to resolve. This reflects a fundamental limitation of monocular perception rather than a deficiency of the proposed framework. Nevertheless, qualitative comparisons on NYUv2 in Fig. 7 show that AMAA produces more coherent and less fragmented structures than the baseline, which is preferable for assistive systems that require stable and predictable feedback.

Thin and distant structures. Extremely thin or distant structures may remain challenging when they occupy only a few pixels and fall below the effective resolution of the encoder hierarchy. AMAA mitigates this issue by selectively propagating informative high-resolution cues through hierarchical adaptive multi-scale fusion, instead of indiscriminately injecting encoder features at all locations. This behavior is supported by the category-wise analysis in Fig. 5, where AMAA exhibits consistently higher median IoU across many indoor object and furniture categories. When discriminative 2D evidence is largely absent, the framework avoids over-confident hallucination, aligning with safety-oriented design principles for visually impaired navigation, where false-negative obstacles are often more hazardous than conservative predictions.

Occlusion, clutter, and distribution shift. In scenes with severe occlusion patterns or clutter configurations that deviate from the training distribution, monocular SSC inevitably relies on learned priors to infer hidden geometry. This may introduce semantic ambiguity or conservative obstacle predictions near traversable space. Despite this, Fig. 7 indicates reduced spurious fragmentation compared with the baseline, and Fig. 6 demonstrates stable training dynamics. These observations suggest that reliability-oriented voxel regulation and gated multi-scale fusion improve robustness without sacrificing optimization stability.

Behavior under real-world deployment conditions. Beyond benchmark evaluation, real-world inference results obtained on the embedded deployment platform (Fig. 8, Fig. 9) further illustrate the practical behavior of the AMAA framework. Under realistic sensing conditions—including

illumination variation, partial occlusion, and camera motion—AMAA preserves continuous free-space boundaries and dominant structural contours. Failure cases in highly reflective or extremely low-texture regions tend to manifest as conservative completion rather than aggressive hallucination. Such behavior is generally preferable for visually impaired assistance, where unstable or oscillatory predictions may translate into misleading or unsafe feedback.

Overall, the observed failure modes are consistent with the inherent ambiguity of monocular 3D inference in complex indoor environments. By explicitly enhancing voxel-feature reliability and regulating cross-scale information flow, the AMAA framework improves structural stability and semantic consistency while remaining suitable for inference-only deployment on embedded assistive platforms. Future work may incorporate uncertainty estimation, temporal consistency, or lightweight multi-frame fusion to further enhance robustness without compromising deployability.

6. Conclusion

This paper presents AMAA, a reliability-oriented monocular semantic scene completion framework that enhances the stability and structural coherence of 3D semantic occupancy prediction under deployable constraints. By explicitly addressing uncertainty introduced by monocular 2D-to-3D lifting and uncontrolled multi-scale feature fusion, the proposed framework improves semantic consistency and reduces structural fragmentation without significantly increasing system complexity.Experimental results on the NYUv2 benchmark demonstrate consistent improvements over a strong monocular baseline. In addition, system-level deployment on an NVIDIA Jetson Orin NX platform and qualitative inference on real-world indoor images verify that the complete AMAA framework can be executed end-to-end on embedded hardware and can generalize beyond curated datasets, supporting its suitability for practical assistive perception scenarios.

Looking forward, substantial opportunities remain for extending monocular 3D perception toward visually impaired assistance. Future work may explore uncertainty-aware reasoning, lightweight temporal integration, and tighter coupling with human-in-the-loop feedback mechanisms, enabling more robust, interpretable, and user-centered assistive navigation systems.

References

[1] World Health Organization, Who publishes the first world vision report, https://www.who.int/zh/news/item/08-10-2019-who-launches-first-world-report-on-vision, accessed: 2026-02-04 (October 2019).

[2] R. N. Kandalan, K. Namuduri, Techniques for constructing indoor navigation systems for the visually impaired: A review, IEEE Transactions on Human-Machine Systems 50 (6) (2020) 492–506.

[3] M. H. Abidi, A. N. Siddiquee, H. Alkhalefah, V. Srivastava, A comprehensive review of navigation systems for visually impaired individuals, Heliyon 10 (11) (2024).

[4] B. Katz, et al., Next-generation navigation assistive tools: A technological review, ACM Computing Surveys 57 (4) (2025) 1–38.

[5] X. Cheng, Geometry-aware contextual reasoning-based indoor accessibility detection system for visually impaired, in: Pattern Recognition and Computer Vision: 8th Chinese Conference, PRCV 2025, Shanghai, China, October 15–18, 2025, Proceedings, Part VI, Springer Nature, 2026, p. 418.

[6] K. Kumar, A. Verma, P. Verma, Visionaid band: real-time smart navigational and alert support system for visually impaired persons using wearable technology, in: 2025 2nd International Conference on Computational Intelligence, Communication Technology and Networking (CICTN), IEEE, 2025, pp. 626–631.

[7] F. Sorgini, R. Caliò, M. C. Carrozza, C. M. Oddo, Haptic-assistive technologies for audition and vision sensory disabilities, Disability and Rehabilitation: Assistive Technology 13 (4) (2018) 394–421.

[8] J. Castiblanco, et al., Technological advancements in human navigation for the visually impaired, Sensors 25 (1) (2025) 124.

[9] C. Jiang, E. Kuang, M. Fan, How can haptic feedback assist people with blind and low vision (blv): A systematic literature review, ACM Transactions on Accessible Computing 18 (1) (2025) 1–57.

[10] L. Roldao, R. De Charette, A. Verroust-Blondet, 3d semantic scene completion: A survey, International Journal of Computer Vision 130 (8) (2022) 1978–2005.

[11] A.-Q. Cao, R. de Charette, Monoscene: Monocular 3d semantic scene completion, in: Proceedings of the IEEE/CVF Conference on Computer Vision and Pattern Recognition (CVPR), 2022, pp. 3991–4001.

[12] Z. Li, W. Wang, H. Li, E. Xie, C. Sima, T. Lu, Q. Yu, J. Dai, Bevformer: learning bird's-eye-view representation from lidar-camera via spatiotemporal transformers, IEEE Transactions on Pattern Analysis and Machine Intelligence (2024).

[13] Y. Huang, W. Zheng, Y. Zhang, J. Zhou, J. Lu, Tri-perspective view for vision-based 3d semantic occupancy prediction, in: Proceedings of the IEEE/CVF conference on computer vision and pattern recognition, 2023, pp. 9223–9232.

[14] X. Wang, Z. Zhu, W. Xu, Y. Zhang, Y. Wei, X. Chi, Y. Ye, D. Du, J. Lu, X. Wang, Openoccupancy: A large scale benchmark for surrounding semantic occupancy perception, in: Proceedings of the IEEE/CVF International Conference on Computer Vision, 2023, pp. 17850–17859.

[15] X. Tian, T. Jiang, L. Yun, Y. Mao, H. Yang, Y. Wang, Y. Wang, H. Zhao, Occ3d: A large-scale 3d occupancy prediction benchmark for autonomous driving, Advances in Neural Information Processing Systems 36 (2023) 64318–64330.

[16] Y. Huang, W. Zheng, B. Zhang, J. Zhou, J. Lu, Selfocc: Self-supervised vision-based 3d occupancy prediction, in: Proceedings of the IEEE/CVF conference on computer vision and pattern recognition, 2024, pp. 19946–19956.

[17] Z. Yu, C. Shu, J. Deng, K. Lu, Z. Liu, J. Yu, D. Yang, H. Li, Y. Chen, Flashocc: Fast and memory-efficient occupancy prediction via channel-to-height plugin, arXiv preprint arXiv:2311.12058 (2023).

[18] H. Li, Y. Hou, X. Xing, Y. Ma, X. Sun, Y. Zhang, Occmamba: Semantic occupancy prediction with state space models, in: Proceedings of the Computer Vision and Pattern Recognition Conference, 2025, pp. 11949–11959.

[19] Y. Tian, S. Bai, Z. Luo, Y. Wang, H. Zhang, B. Guo, Y. Lv, F.-Y. Wang, Mambaocc: Visual state space models for bev-based occupancy prediction with local adaptive reordering, Expert Systems with Applications (2026) 131305.

[20] X. Wang, W. Feng, L. Wan, Multi-modal fusion architecture search for camera-based semantic scene completion, Expert Systems with Applications 243 (2024) 122885.

[21] H. Yu, Y. Wang, Y. Chen, Z. Zhang, Monocular occupancy prediction for scalable indoor scenes, in: European Conference on Computer Vision, Springer, 2024, pp. 38–54.

[22] J. Li, M. Lu, J. Liu, H. Wang, C. Gu, W. Zheng, L. Du, S. Zhang, Sliceocc: Indoor 3d semantic occupancy prediction with vertical slice representation, in: 2025 IEEE International Conference on Robotics and Automation (ICRA), IEEE, 2025, pp. 15762–15768.

[23] Y. Wu, W. Zheng, S. Zuo, Y. Huang, J. Zhou, J. Lu, Embodiedocc: Embodied 3d occupancy prediction for vision-based online scene understanding, in: Proceedings of the IEEE/CVF International Conference on Computer Vision, 2025, pp. 26360–26370.

[24] H. Wang, X. Wei, X. Zhang, J. Li, C. Bai, Y. Li, M. Lu, W. Zheng, S. Zhang, Embodiedocc++: Boosting embodied 3d occupancy prediction with plane regularization and uncertainty sampler, in: Proceedings of the 33rd ACM International Conference on Multimedia, 2025, pp. 925–934.

[25] X. Tan, W. Wu, Z. Zhang, C. Fan, Y. Peng, Z. Zhang, Y. Xie, L. Ma, Geocc: Geometrically enhanced 3d occupancy network with implicit-explicit depth fusion and contextual self-supervision, IEEE Transactions on Intelligent Transportation Systems (2025).

[26] F. Wang, Q. Sun, D. Zhang, J. Tang, Unleashing network potentials for semantic scene completion, in: Proceedings of the IEEE/CVF Conference on Computer Vision and Pattern Recognition, 2024, pp. 10314–10323.

[27] H. Cao, S. Behnke, Diffssc: Semantic lidar scan completion using denoising diffusion probabilistic models, in: 2025 IEEE/RSJ International Conference on Intelligent Robots and Systems (IROS), IEEE, 2025, pp. 2185–2192.

[28] Y. Wang, Y. Liu, T. Yuan, Y. Mao, Y. Liang, X. Yang, H. Zhang, H. Zhao, Diffusion-based generative models for 3d occupancy prediction in autonomous driving, arXiv preprint arXiv:2505.23115 (2025).

[29] H. Lu, Y. Su, X. Zhang, L. Gao, Y. Xue, L. Wang, Vishall3d: Monocular semantic scene completion from reconstructing the visible regions to hallucinating the invisible regions, in: Proceedings of the IEEE/CVF International Conference on Computer Vision, 2025, pp. 28674–28684.

[30] N. Hughes, Y. Chang, L. Carlone, Hydra: A real-time spatial perception system for 3d scene graph construction and optimization, arXiv preprint arXiv:2201.13360 (2022).

[31] H. Hakim, A. Fadhil, Indoor wearable navigation system using 2d slam based on rgb-d camera for visually impaired people, in: Proceedings of First International Conference on Mathematical Modeling and Computational Science: ICMMCS 2020, Springer, 2021, pp. 661–672.

[32] H. Zhang, L. Jin, C. Ye, An rgb-d camera based visual positioning system for assistive navigation by a robotic navigation aid, IEEE/CAA Journal of Automatica Sinica 8 (8) (2021) 1389–1400.

[33] Y. Song, Z. Li, G. Li, B. Wang, M. Zhu, P. Shi, Multi-sensory visual-auditory fusion of wearable navigation assistance for people with impaired vision, IEEE Transactions on Automation Science and Engineering (2023).

[34] E. Casanova, D. Guffanti, L. Hidalgo, Technological advancements in human navigation for the visually impaired: A systematic review, Sensors 25 (7) (2025) 2213.

[35] R. Pal, S. Kar, D. K. Prasad, A. A. Sekh, Visionaidqa: Advancing visual question answering for the visually impaired, ACM Computing Surveys (2026).

[36] C. H. Song, J. Wu, C. Washington, B. M. Sadler, W.-L. Chao, Y. Su, Llm-planner: Few-shot grounded planning for embodied agents with large language models, in: Proceedings of the IEEE/CVF international conference on computer vision, 2023, pp. 2998–3009.

[37] H. Ye, C.-J. Lee, T.-Y. Wu, X.-D. Yang, B.-Y. Chen, R.-H. Liang, Body-centric nfc: Body-centric interaction with nfc devices through near-field enabled clothing, in: Proceedings of the 2022 ACM Designing Interactive Systems Conference, 2022, pp. 1626–1639.

[38] V. Kachurka, B. Rault, F. I. I. Muñoz, D. Roussel, F. Bonardi, J.-Y. Didier, H. Hadj-Abdelkader, S. Bouchafa, P. Alliez, M. Robin, Wecoslam: Wearable cooperative slam system for real-time indoor localization under challenging conditions, IEEE Sensors Journal 22 (6) (2021) 5122–5132.

[39] Y. Zhang, Z. Zhu, D. Du, Occformer: Dual-path transformer for vision-based 3d semantic occupancy prediction, in: Proceedings of the IEEE/CVF International Conference on Computer Vision, 2023, pp. 9433–9443.

[40] Y. Huang, W. Zheng, Y. Zhang, J. Zhou, J. Lu, Gaussianformer: Scene as gaussians for vision-based 3d semantic occupancy prediction, in: European Conference on Computer Vision, Springer, 2024, pp. 376–393.

[41] F. Ding, X. Wen, Y. Zhu, Y. Li, C. X. Lu, Radarocc: Robust 3d occupancy prediction with 4d imaging radar, Advances in Neural Information Processing Systems 37 (2024) 101589–101617.

[42] L. Kong, Y. Liu, X. Li, R. Chen, W. Zhang, J. Ren, L. Pan, K. Chen, Z. Liu, Robo3d: Towards robust and reliable 3d perception against corruptions, in: Proceedings of the IEEE/CVF International Conference on Computer Vision, 2023, pp. 19994–20006.

[43] J. Kim, C. Kang, D. Lee, S. Choi, J. W. Choi, Protoocc: Accurate, efficient 3d occupancy prediction using dual branch encoder-prototype query decoder, in: Proceedings of the AAAI Conference on Artificial Intelligence, Vol. 39, 2025, pp. 4284–4292.

[44] L. Liang, N. Akhtar, J. Vice, X. Kong, A. S. Mian, Skip mamba diffusion for monocular 3d semantic scene completion, in: Proceedings of the AAAI Conference on Artificial Intelligence, Vol. 39, 2025, pp. 5155–5163.

[45] Y. Li, Z. Yu, C. Choy, C. Xiao, J. M. Alvarez, S. Fidler, C. Feng, A. Anandkumar, Voxformer: Sparse voxel transformer for camera-based 3d semantic scene completion, in: Proceedings of the IEEE/CVF conference on computer vision and pattern recognition, 2023, pp. 9087–9098.

[46] S. Zeng, W. Zheng, J. Lu, H. Yan, Hardness-aware scene synthesis for semi-supervised 3d object detection, IEEE Transactions on Multimedia 26 (2024) 9644–9656.

[47] B. Li, J. Deng, Y. Sun, X. Wang, X. Jin, W. Zeng, Hierarchical context alignment with disentangled geometric and temporal modeling for semantic occupancy prediction, IEEE Transactions on Pattern Analysis and Machine Intelligence (2026).

[48] C. Zhang, J. Yan, Y. Wei, J. Li, L. Liu, Y. Tang, Y. Duan, J. Lu, Occnerf: Advancing 3d occupancy prediction in lidar-free environments, IEEE Transactions on Image Processing (2025).

[49] A. Vobecky, O. Siméoni, D. Hurych, S. Gidaris, A. Bursuc, P. Pérez, J. Sivic, Pop-3d: Open-vocabulary 3d occupancy prediction from images, Advances in Neural Information Processing Systems 36 (2023) 50545–50557.

[50] J. Pan, Z. Wang, L. Wang, Co-occ: Coupling explicit feature fusion with volume rendering regularization for multi-modal 3d semantic occupancy prediction, IEEE Robotics and Automation Letters 9 (6) (2024) 5687–5694.

[51] W. Zheng, W. Chen, Y. Huang, B. Zhang, Y. Duan, J. Lu, Occworld: Learning a 3d occupancy world model for autonomous driving, in: European conference on computer vision, Springer, 2024, pp. 55–72.

[52] H. Xiao, H. Xu, W. Kang, Y. Li, Instance-aware monocular 3d semantic scene completion, IEEE Transactions on Intelligent Transportation Systems 25 (7) (2024) 6543–6554.

[53] Y. Kwon, W. Kim, H. Kim, Hard: Hardware-aware lightweight real-time semantic segmentation model deployable from edge to gpu, in: Proceedings of the Asian Conference on Computer Vision, 2024, pp. 3552–3569.

[54] Z. Dou, D. Ye, B. Wang, Autosegedge: Searching for the edge device real-time semantic segmentation based on multi-task learning, Image and Vision Computing 136 (2023) 104719.

[55] H.-H. Nguyen, D. N.-N. Tran, J. W. Jeon, Real-time semantic segmentation on edge devices with nvidia jetson agx xavier, in: 2022 IEEE international conference on consumer electronics-Asia (ICCE-Asia), IEEE, 2022, pp. 1–4.

[56] J. Zhang, Y. Zhang, Q. Liu, Y. Wang, Lightweight spatial embedding for vision-based 3d occupancy prediction, arXiv preprint arXiv:2412.05976 (2024).

[57] S. Yuan, J. Wei, M. Tie, X. Ren, Z. Gan, W. Ding, Lmpocc: 3d semantic occupancy prediction utilizing long-term memory prior from historical traversals, arXiv preprint arXiv:2504.13596 (2025).

[58] N. Silberman, D. Hoiem, P. Kohli, R. Fergus, Indoor segmentation and support inference from rgbd images, in: Proceedings of the

European Conference on Computer Vision (ECCV), 2012, pp. 746–760.

[59] S. Song, F. Yu, A. Zeng, A. X. Chang, M. Savva, T. Funkhouser, Semantic scene completion from a single depth image, in: Proceedings of the IEEE conference on computer vision and pattern recognition, 2017, pp. 1746–1754.

[60] L. Roldao, R. De Charette, A. Verroust-Blondet, Lmscnet: Lightweight multiscale 3d semantic completion, in: 2020 International Conference on 3D Vision (3DV), IEEE, 2020, pp. 111–119.

[61] J. Li, Y. Liu, D. Gong, Q. Yuan, Anisotropic convolutional networks for 3d semantic scene completion, in: Proceedings of the IEEE/CVF Conference on Computer Vision and Pattern Recognition (CVPR), 2020, pp. 3351–3359.

[62] X. Chen, K.-Y. Lin, C. Wang, W. Zeng, H. Li, 3d sketch-aware semantic scene completion via semi-supervised structure prior, in: Proceedings of the IEEE/CVF Conference on Computer Vision and Pattern Recognition (CVPR), 2020, pp. 4193–4202.